JOURNAL OF GEOPHYSICAL RESEARCH, VOL. ???, XXXX, DOI:10.1029/,

Compaction of porous rock by dissolution on discrete stylolites: a one-dimensional model

Luiza Angheluta[1], Joachim Mathiesen[1,2], Einat Aharonov[3]

Luiza Angheluta, Physics of Geological Processes, University of Oslo, box 1047, *0316* Blindern, Norway

Joachim Mathiesen, Niels Bohr Institute, University of Copenhagen, Denmark, mathies@nbi.dk

Einat Aharonov, The Hebrew University in Jerusalem, Earth Science Institute, Israel

[1]Physics of Geological Processes,
University of Oslo, Norway.

[2]Niels Bohr Institute, University of
Copenhagen, Denmark.

[3]The Hebrew University in Jerusalem,
The Fredy and Nadine Herrmann Institute
of Earth Sciences, Israel.

Abstract. Compaction of sedimentary porous rock by dissolution and precipitation is a complex deformation mechanism, that is often localized on stylolites and pressure solution seams. We consider a one-dimensional model of compaction near a thin clay-rich stylolite embedded in a porous rock. Under the assumption that the clay enhances solubility, the model predicts a reactive transport away from the clay layer followed by pore cementation. The evolution of the porosity, reactant transport, and compaction rate are studied as functions of model parameters and shown to reach a stationary state. We find good agreement between the porosity distribution predicted by the model and previously reported field measurements. The model provides quantitative estimates for compaction rates on stylolitic surfaces.

1. Introduction

Pressure solution is a major ductile deformation mechanism operating in sedimentary rocks [*Weyl*, 1959], with practical implications to oil, gas, and water flows, as well as to controlling rates of basic geological processes such as rock compaction [*Dewers and Ortoleva*, 1990], folding [*McClay*, 1977], and frictional healing of faults [*Yasuhara et al.*, 2005; *Renard et al.*, 2000]. The premise of the pressure solution phenomenon is that 'pressure' , or 'stress' , is the critical driving force for mass transfer creep where material dissolution occurs in regions experiencing high stress, followed by ionic diffusion through a fluid-saturated pore space, and precipitation in regions of low stress. The pressure solution process is believed to spontaneously yield localized patterns, such as pressure solution seams (PSS) and stylolites. Stylolites differ from the rather smooth PSS by their serrated 'teeth', that grow sub-parallel to the direction of compaction, see e.g. [*Rutter*, 1983]. Several mechanisms have been proposed to explain the localization and growth of stylolites and PSS: i) propagation of anticracks [*Fletcher and Pollard*, 1981], ii) a porosity-dissolution feedback [*Merino et al.*, 1983], and more recently, iii) an enhancement of pressure solution due to clays [*Wangen*, 1998; *Aharonov and Katsman*, 2009]. In addition, various mechanisms have been suggested for the roughening of stylolites from an initial flat surface, such as pinning of passive markers during compaction coupled with long range correlations [*Koehn et al.*, 2007; *Ebner et al.*, 2009; *Schmittbuhl et al.*, 2004a, b], a strain energy induced instability [*Gal et al.*, 1998; *Dysthe et al.*, 2006; *Misbah et al.*, 2004], or a mechanical instability caused by gradients in material properties [*Angheluta et al.*, 2008, 2010].

Recent experimental studies challenge the premise that the pressure solution process is solely driven by the effect of 'pressure', and consider dissolution in the presence of clays or other materials [*Greene et al.*, 2009; *Kristiansen et al.*, 2011]. The presence of clays in sedimentary rocks has been observed to enhance dissolution of minerals, both in quartz and in carbonates (e.g. [*Bjorkum*, 1996; *Marshak and Engelder*, 1985; *Sibley and Blatt*, 1976; *Heald*, 1959]). In addition to field observations, experiments also show a significant increase in the compaction rate owing to clays, both for halite [*Hickman and Evans*, 1995; *Renard et al.*, 1997, 2001] and for quartz sand [*Rutter and Wanten*, 2000]. The importance of clays in the pressure solution process is further evidenced by the fact that stylolites often appear in conjunction with certain types of clays [*Walderhaug et al.*, 2006; *Thomson*, 1959], and that stylolites are observed to initiate from clay-rich surfaces [*Walderhaug and Bjorkum*, 2003; *Tada and Siever*, 1989]. Numerical modeling [*Fueten et al.*, 2002; *Aharonov and Katsman*, 2009; *Katsman et al.*, 2006] also suggests that the enhancement of pressure solution by clays may be essential for the localization and growth of stylolites.

Though several mechanisms have been proposed for the evolution of porosity in reactive rocks that experience pressure solution [*Wangen*, 1998; *Renard et al.*, 2001; *Walderhaug et al.*, 2004, 2006], the controlling factors for mineral dissolution are still debated. Recent studies suggest that a pore-size controlled mineral solubility of the rock is an important factor in the porosity reduction adjacent to isolated stylolite, regardless of the presence of clays [*Emmanuel et al.*, 2009, 2010]. Alternatively, the premise that stylolites are seams of higher solubility, has been used in models where the pore fluid in contact with a stylolite has a local equilibrium of the solute concentration c_{eq}^{i} that is higher than the equilibrium concentration c_{eq}^{∞} in the pore fluid near the soluble rock minerals away from the stylolite [*Bjorkum*, 1996; *Wangen*, 1998, 1999; *Oelkers et al.*, 1996]. This causes dissolution to localize on the high solubility surface with concurrent precipitation within the bulk rock adjacent to it. Field evidence, including stylolites that develop in uniform structures parallel to the sedimentary bedding and extend spatially over more than 1 km [*Laronne Ben-Itzhak et al.*, 2012; *Safaricz and Davison*, 2005], and stylolites that develop in association with the initial distribution of clays (and other mineralogical heterogeneities) [*Lind*, 1993; *Marshak and Engelder*, 1985; *Thomson*, 1959], support the above hypothesis that PSS and stylolite localization may be driven by a preexisting chemical heterogeneity. Yet, to the best of our knowledge there are no experimental measurements that quantify the enhanced equilibrium concentration due to the presence of mineralogical heterogeneity such as clays.

In this paper, we investigate a model of local compaction of a fluid-saturated, porous rock due to dissolution on an isolated clay-rich stylolite, and precipitation away from it. We assume a jump in the mineral solubility, with a higher value at the stylolite interface than in the bulk of the rock. This leads to dissolution in the mineral adjacent to the stylolite, and precipitation everywhere else. The higher solubility is here considered to be due to chemical heterogeneities, however, other reasons for higher solubility, e.g. higher stress due to higher porosity [*Merino et al.*, 1983], are expected to lead to similar results. We study the evolution of porosity and concentration profiles away from the stylolite in relation to the existing porosity measurements. The rest of the paper is organized as follows: In Section 2, we formulate a one-dimensional model of reactive transport coupled with compaction and analyze it further in Section 3. The numerical results and a comparison with field measurements of the porosity profile is presented in Section 4, and concluding remarks are summarized in Section 5.

2. Model formulation:

For simplicity, we idealize the system by neglecting the effect of surface morphology as well as stress-induced surface dissolution, and study the effect of an increased mineral solubility due to clays. Thus, we consider a one-dimensional model of a fluid-saturated, monomineralic porous rock with a pre-existing flat clay-rich stylolite. The pore fluid has a soluble component with a mass concentration $c(x,t)$, i.e. mass fraction. The equilibrium concentration of solute in the pore fluid at the contact with the clay is $c^i_{eq}(x,t)$. In other parts of the rock, the equilibrium concentration is lower and equal to $c^\infty_{eq}(x,t)$.

Changes in porosity can occur by local precipitation in areas of supersaturation as well as by mechanical deformation. The former mechanism for pore evolution is also known as chemical compaction, whereas the latter typically refers to mechanical compaction. In nature, both of these mechanisms may operate at the same time, however, in models these regimes are often studied separately in order to achieve a better understanding of each individual regime. In what follows, we focus on the porosity change due to precipitation away from a dissolution front, thus we neglect the role of mechanical deformation.

The evolution of porosity $\phi(x,t)$ and concentration $c(x,t)$ away from a stylolite interface is determined from the balance law of mass in the solid phase and fluid phase,

$$\rho_f \frac{\partial(\phi c)}{\partial t} - \frac{\partial}{\partial x}\left[\phi \rho_f D(\phi)\frac{\partial c}{\partial x}\right] = -R_b(\phi)(c - c^\infty_{eq}) \qquad (1)$$

$$\rho_s \frac{\partial(1-\phi)}{\partial t} + \frac{\partial}{\partial x}\left[v_s \rho_s (1-\phi)\right] = R_b(\phi)(c - c^\infty_{eq}), \qquad (2)$$

where v_s is the local 'collapse' velocity of the porous solid, ρ_f is the mass density of the fluid, ρ_s is the mass density of the solid, $D(\phi)$ is the diffusion constant for the solute as function of porosity, $R_b(\phi)$ is the bulk reaction coefficient from a linear reaction kinetics, and c_{eq}^{∞} is the far-field solute equilibrium concentration in the porous rock. These equations are similar to the mass balance formulations for reactive transport in porous media [*Steefel and Lasaga*, 1994; *Aharonov et al.*, 1997], except for the additional advective term in Eq. (2) which accounts for the collapse of the porous structure due to dissolution at the stylolite. Eq. (1) describes the diffusion transport of the dissolved component in the pore space and precipitation when the pore fluid is supersaturated. Due to the higher solubility at the stylolitic surface, local dissolution will occur, followed by solute diffusion, and porosity reduction by precipitation in the bulk rock. The continued discharge from the dissolution interface stimulates an ongoing cementation of the pores in the surrounding solid. Moreover, because of surface dissolution, the porous structure is rigidly moving towards the stylolite with a collapse velocity v_s, which, in the absence of deformation due to gravity or imposed stress, is determined by the interfacial dissolution rate. The evolution of porosity away from the stylolite, as expressed by Eq. (2), is due to precipitation in regions with supersaturation and advection of rigid pore structure towards the dissolution site.

Solutions to Eqs. (1)-(2) are determined from the boundary conditions for the concentration and solid velocity. The concentration field far away from the stylolite reaches the equilibrium concentration $c(+\infty) = c_{eq}^{\infty}$. At the contact with the stylolite, located at $x = 0$, the equilibrium concentration is elevated and leads to local dissolution. Mass balance at the interface requires that the amount of dissolved component is diffused into the pore space, namely

$$\rho_f \phi D(\phi) \frac{\partial c}{\partial x}|_{x=0} = R_i(\phi)(c - c_{eq}^i)|_{x=0}, \tag{3}$$

where $x = 0$ represents the contact with a clay-rich stylolite, $R_i(\phi)$ is the surface reaction rate, and $c_{eq}^i > c_{eq}^\infty$ is the elevated equilibrium concentration at $x = 0$. The collapse velocity at the interface is assumed to be proportional to the dissolution kinetics

$$(1-\phi)\rho_s v_s|_{x=0} \; = \; bR_i(\phi)(c - c_{eq}^i)|_{x=0}, \tag{4}$$

where b is the stoichiometric constant.

A recently proposed one-dimensional model also investigates the evolution of the porosity neighboring a stylolite surface [*Emmanuel et al.*, 2009, 2010]. However, in their model, a pore-size controlled solubility (PCS) is assumed, while in our model the initial porosity is uniform and the increased solubility is determined by the presence of clays. Also, in the PCS model, the dissolution at an isolated stylolite is modelled as a moving boundary problem, whereas, in our setup, the dissolution surface is stationary while the pore structure moves towards it with a speed determined by the interfacial dissolution rate. In PCS model the pore fluid is stationary in the absence of externally imposed flow. We believe that, as a consequence of the moving dissolution front, there will be an effective pore fluid advection with a velocity determined by the dissolution rate when the porous skeleton of the rock is static.

2.1. Dimensional analysis

The diffusion coefficient and reaction rates depend on the local porosity by empirical laws, which are typically on the form $D(\phi) = D_0\phi^2$, $R_i(\phi) = R_i^0\phi$ and $R_b(\phi) = R_b^0\phi$ [*Zhao et al.*, 2008]. In the present formulation, the bulk reaction rate R_b^0 is measured in units of $[R_b^0] = 1$ kg/(m^3 s), while the dissolution rate at the interface R_i^0 has units of $[R_i^0] = 1$ kg/(m^{2}s) [*Aharonov et al.*, 1997]. The different units in the kinetic rates R_b^0 and R_i^0 are directly related to the different reactive areas in the bulk and at a surface. Namely, we can write the kinetic rates as $R_{b,i}^0 = \rho_s k_{b,i} A_{b,i}$, where $k_{b,i}$ is the reactive rate constant of the soluble component given in units of $[k_{b,i}] = 1$ m/s and $A_{b,i}$ is the effective area available for reaction. Thus, $[A_b] = 1$ m^2/m^3 is defined per unit volume and $[A_i] = 1$ m^2/m^2 is measured per unit surface area.

From the diffusion coefficient and bulk precipitation rate, we define a characteristic time-scale of precipitation and a length-scale of the diffusion before precipitation

$$t_0 = \frac{\rho_f}{R_b^0}, \qquad x_0 = \sqrt{\frac{D_0 \rho_f}{R_b^0}}. \tag{5}$$

Time and space is then rescaled with these typical units, i.e. $\tilde{t} \equiv t/t_0$ and $\tilde{x} \equiv x/x_0$. The typical speed, associated with diffusion and precipitation, is thus measured in units of $v_0 = x_0/t_0 = \sqrt{D_0 R_b^0/\rho_f}$ and $\tilde{v}_s \equiv v_s/v_0$. We also rescale the concentration relative to the far field equilibrium concentration c_{eq}^∞ so that $u = (c - c_{eq}^\infty)/c_{eq}^\infty$ and $u_\infty = 0$. Our assumption is that the equilibrium concentration is elevated near the stylolite, *i.e.* $c_{eq}^i = c_{eq}^\infty(1 + \Delta)$ with $\Delta > 0$.

In the remaining text, we drop the tilde symbol over rescaled quantities. Furthermore, the $\phi(x,t)$ and $c(x,t)$ fields are determined from the non-dimensional versions of Eqs. (1)-(2)

$$\frac{\partial(\phi u)}{\partial t} - \frac{\partial}{\partial x}\left[\phi^3 \frac{\partial u}{\partial x}\right] = -\phi u \tag{6}$$

$$\frac{\partial \phi}{\partial t} + \frac{\partial}{\partial x}\left(v_s \phi\right) = -\epsilon \phi u, \tag{7}$$

where $\epsilon = c_{eq}^{\infty}\rho_f/\rho_s$. The interfacial boundary conditions become

$$\begin{aligned} \phi^3 \frac{\partial u}{\partial x}|_{x=0} &= \beta\epsilon^{-1}\phi(u-\Delta)|_{x=0} && (8) \\ (1-\phi)v_s|_{x=0} &= b\beta\phi(u-\Delta)|_{x=0}, && (9) \end{aligned}$$

where the interfacial velocity v_s is measured in typical units of v_0. Here $\beta = R_i^0 c_{eq}^{\infty}/(v_0\rho_s)$ is the surface dissolution rate relative to the bulk diffusion and precipitation. Using the definition of v_0 from above, the parameter β can also be expressed equivalently as $\beta = k_i A_i c_{eq}^{\infty}/\sqrt{D_0 k_b A_b}$.

2.2. Parameter values for porous rocks

The dynamics is controlled by several non-dimensionless variables such as ϵ, b, Δ and β, some of which can be fixed by material properties. As an example, we consider sedimentary porous rock composed by either quartz, e.g. sandstones, or calcite, e.g. limestones.

The parameter ϵ is determined by the ratio of the fluid to solid density times the equilibrium mass fraction of the soluble component. As an order of magnitude estimate, typical solubilities in mass fraction for quartz range between $0.6 - 60 \times 10^{-5}$, depending on conditions (temperature, grain size) [*Hem*, 1985]. For calcite the solubility ranges, depending on conditions, mostly between $c_{eq}^{\infty} \sim 4 - 100 \times 10^{-5}$ mass fractions [*Coto et al.*, 2012]. Since the ratio between fluid and solid density is roughly 0.4, ϵ varies between $0.6 - 100 \times 10^{-5}$. We consider $\epsilon = 4 \times 10^{-5}$ as a typical value, but other values within the variability range give similar results.

We assume a uniform background porosity as typically given by $\phi^{\infty} = 0.2$ and set the stoichiometric constant $b = 1$. Hence, we are left with two varying parameters Δ and β.

The relative supersaturation Δ is somewhat harder to determine. Petrographic studies on quartz suggest that the degree of supersaturation away from the stylolites could be of the order of 0.01 [*Wangen*, 1999]. The value has not yet been documented for other rock types. However, since the value may vary for other rock systems, we study the dependency of the porosity and concentration gradients, as well as the steady state collapse velocity on the different values of Δ in the range $10^{-2} - 10^{-1}$.

The other varying parameter β represents the surface kinetics rate relative to bulk diffusion. While the diffusion coefficient is roughly $D \sim 10^{-9}$ m^2/s for both quartz and calcite, the bulk and surface reaction rates may vary over several orders of magnitude. With the typical rock values listed in Table 2, we find that the bulk reaction rate for quartz is typically in the range of $R_b^0 \sim 2.6 \times 10^{-5}$ kg/(m^3 s), and it can vary between $10^{-4} - 10^{-1}$ kg/(m^3 s) for calcites. The interfacial kinetics rates are typically of the order of $R_i^0 \sim 10^{-6} - 10^{-4}$ kg/(m^2 s) for quartz and $R_i^0 \sim 10^{-5} - 10^{0}$ kg/(m^2 s) for calcite. Hence, β varies between $10^{-6} - 10^{-2}$ for quartz and for calcite $\beta \sim 10^{-7} - 10^{2}$. Using the values for the parameters from Table 2, we can also estimate the typical units $t_0 \sim 1$ yr, $x_0 \sim 0.2$ m and $v_0 \sim 0.2$ m/yr for quartz. For calcite t_0 ranges from 3 hrs to 30 days, $x_0 \sim 1 - 10$ cm and $v_0 \sim 0.5 - 100$ m/yr for calcite.

3. Chemical compaction

The Eqs. (6)-(7) can be equivalently rewritten as

$$\frac{\partial \phi}{\partial t} + v_s \frac{\partial \phi}{\partial x} = -\epsilon \phi u \tag{10}$$

$$\phi \frac{\partial u}{\partial t} = \frac{\partial}{\partial x}\left(\phi^3 \frac{\partial u}{\partial x}\right) + \phi(\epsilon u^2 - u), \tag{11}$$

where the velocity of the solid is determined from the interfacial condition

$$v_s = \beta \frac{\phi(u-\Delta)}{1-\phi}\big|_{x=0}. \tag{12}$$

The concentration field satisfies the far field equilibrium condition $u(+\infty) = 0$ and mass balance at the interface

$$\phi^2 \frac{\partial u(x)}{\partial x}\big|_{x=0} = \beta\epsilon^{-1}(u-\Delta)\big|_{x=0}. \tag{13}$$

3.1. Asymptotic solution

The long time solution is characterized by a uniform collapse rate of the solid and by stationary porosity and concentration fields. In this asymptotic steady state regime, the time-dependent part of Eqs. (10)-(11) can be dropped

$$v_s\phi' + \epsilon\phi u \ = \ 0 \tag{14}$$

$$3\phi\phi' u' + \phi^2 u'' + \epsilon u^2 - u \ = \ 0, \tag{15}$$

where $u' \equiv du/dx$ and $\phi' \equiv d\phi/dx$. By substituting ϕ' from Eq. (14) into Eq. (15), we arrive at

$$\phi^2 u'' - u + \epsilon\left(u^2 - \frac{3\phi^2}{v_s}uu'\right) \ = \ 0,. \tag{16}$$

For typical parameter values for rocks, we can safely assume that $\epsilon \ll 1$, in which case the above equation simplifies to

$$\phi_0^2 u'' - u \ \approx \ 0, \tag{17}$$

when we neglected the corrections due to a steep porosity gradient near the interface. The asymptotic solution satisfying the interfacial and far-field boundary conditions is given by

$$u(x) \approx \Delta e^{-x/\phi_0}. \tag{18}$$

The numerical solution without any of these approximations follows nicely the exponential decay away from the interface as shown in Fig. (1) panel (b). Near the dissolution site where the gradient in porosity becomes important, the numerical solution deviates from the asymptotic trend such that the concentration decays initially faster than exponential. Inserting this exponential solution of $u(x)$ into Eq. (14), we find that

$$\phi(x) \approx \phi_0 \exp\left(-\epsilon\phi_0\Delta \exp\left(-x/\phi_0\right)\right). \tag{19}$$

This approximate solution is compared with the numerical solution of Eqs. (10)-(11) and the result is shown in panel (a) of Fig. (1). The asymptotic solution provides an accurate description of the porosity profile almost everywhere except very close to the interface where it slightly overestimates the minimum attained porosity. This is because, near the interface, the concentration gradient is steeper than predicted by the asymptotic solution, hence the transport of mass away from the interface and the immediate precipitation are enhanced.

4. Numerical results

We integrate numerically Eqs. (10)-(11) and compare the results with a porosity profile found in field measurements. The numerical integration scheme is explained in detail in the Appendix.

Using typical parameter values for sandstones (see Table 2), we compare the measurements of porosity reduction in the vicinity of stylolites from sandstone samples taken from the Stø Formation in the Barents Sea (data from [*Emmanuel et al.*, 2010]) with the steady state profile obtained from our model. We find that our model fits very well the steep gradient in porosity near a dissolution surface as shown in Fig. (2). Moreover, we find that the asymptotic solution of the stationary $\phi(x)$ is independent of β, although the associated relaxation timescale is different for different values of β. Also, the dependence on Δ is not significant given that Δ is of the order of 10^{-2}. Thus, we conclude that the stationary $\phi(x)$ is relatively stable for different values of Δ and β, but the timescale on which this state is approached is strongly determined by the dimensionless numbers of the model.

In Fig. 3, we show the transitory dynamics of the porosity and concentration fields as the steady state compaction is approached using the typical parameter values for sandstone sediments. Since the far-field porosity ϕ_0 is uniform, we have superimposed a Gaussian peak with higher porosity so that we can visualize how much the solid has collapsed by the motion of the peak towards the interface. The high porosity peak is located sufficiently far away from the interface, such that the local porosity gradients of the peak do not affect the diffusion and precipitation in the region near the dissolution site. Steeper gradients in $\phi(x,t)$ and $u(x,t)$ are localized on a length-scale smaller than or comparable with x_0, while on larger length-scales, the porosity becomes uniform and the concentration decays according to the exponential far-field solution. We also notice, that at early times $u(x,t)$ is very well approximated by the exponential solution, and, as the porosity starts to change near the interface due to local precipitation, the concentration field also decays much faster nearby. In the late stages of evolution, the velocity v_s approaches a constant value for a given β, corresponding to a steady state compaction. In this regime, the concentration and porosity profiles become time independent.

We also note that the relaxation time to the steady state diverges as β, *i.e.* the rate of dissolution relative to the bulk diffusion and precipitation, is decreased. The solid collapses faster at the beginning and slows down to a constant velocity in the steady state. For very small values of β, the collapse velocity v_s depends on β as shown in Fig. (4 a)) and saturates at an independent constant value for higher β's. This is because at larger values of β, the system relaxes much faster to the stationary profile of ϕ and u, and proceeds from there on with a velocity that is determined by the mass transport away from the interface. A similar behaviour is observed also by varying the supersaturation parameter Δ. With increasing Δ, the collapse velocity also increases initially but it saturates to value that becomes asymptotically independent of Δ's and β's as shown also in the contour plot of $|v_s|$ as a function of these two varying parameters in Fig. (4 b)). The high β's and Δ's regime corresponds to a diffusion limited dynamics where the collapse rate is determined by the diffusion transport rather then by the dissolution rate at the interface.

From numerical simulations, we observe that porosity changes away from the dissolution surface are relatively robust with varying β and Δ. The concentration at the dissolution point is smaller but proportional to Δ. Upon, rescaling $u(x)$ with its value at $x = 0$, the concentration has a universal profile away from the interface with an exponential decay sufficiently far away from the $x = 0$. This is shown in Fig. (1) and is consistent with the fact that the asymptotic solutions are independent of β.

5. Discussion and conclusions

We have studied the effect of a solubility jump on the spatial distribution of porosity and solute concentration in a porous rock. In particular, we analysed the situation where dissolution occurs on an isolated, clay-rich stylolite. This situation leads to a steady state chemical compaction driven by local dissolution, mass transport by diffusion through the pore space and precipitation away from the stylolite.

In the steady state, the pore space near the interface is not fully clogged allowing for a continuous dissolution. We have found that away from the stylolite, the solute concentration relaxes exponentially to the far field bulk equilibrium solution, while the porosity approaches a uniform value according to a double exponential function in agreement with the asymptotic analytical solution. However, in the vicinity of the dissolution surface, the concentration and porosity profiles are characterized by steeper gradients then the asymptotic predictions. The concentration and porosity high gradients are localized on a distance comparable to the characteristic diffusion length-scale x_0 on the precipitation time-scale, thus it depends on the diffusivity and kinetics rate as $x_0 = \sqrt{D_0 \rho_f / R_b^0}$. The system relaxes to a steady state collapse rate, where $\phi(x)$ and $u(x)$ approach stationary distributions. The stationary profiles are relatively robust over a wide range of parameter values of Δ and β (Fig. 3). However, the collapse rate and the relaxation time-scale to the steady state depend on the values of the model parameters as shown in Fig. 4. The typical collapse rates v_s in the steady state are of the order of $10^{-4} - 10^{-3}$ m/Myr for quartz and between 10^{-3} and 1 m/Myr for calcite. The lower values are expected to apply closer to the surface, with rates increasing to the higher values with temperature and burial depth.

The collapse rates we predict are very low: the rates of porous rock compaction, which are also the rates at which stylolites grow, are about a million times slower than the rate constants k_i for mineral interface dissolution measured under lab conditions. The slowness is associated to the fact that our relevant parameter values for calcite and quartz predict a porosity evolution in a diffusion-precipitation limited regime. Such rates may explain why stylolites were never observed in the lab. These results agree well with the size of stylolite's 'teeth'. Taking the Stø formation as an example, the formation is lower Jurassic, i.e. around 170-190 Myrs old. Cores of stylolites extracted from this formation show 'teeth' of about few cm in amplitude [*Walderhaug et al.*, 2006], indicating more than a few cm of dissolution. If we denote the amount of dissolution on each stylolite as $L \sim 0.05m$, we predict that the time for its development is $t_d = L/v_s$. Using our inferred quartz collapse rate, $v_s \sim 10^{-3}$ m/Myr, we conclude that the Stø stylolites developed over $t_d = 50$ million yrs. Our predicted v_s for quartz also explains why stylolites in quartz are mainly found at depths exceeding 1.5 km burial [*Tada and Siever*, 1989]. Namely, observable 'teeth' (i.e. $L \sim 0.01m$) develop over at least 10 Myrs, and, assuming a burial rate of 10 Myr/km, it provides an estimate for a minimum observed depth for initial stylolitization in siliciclastic rocks. In contrast, stylolites in calcite form as shallow as 90 meters [*Tada and Siever*, 1989], or even less. We find that v_s in calcite is up to 3 orders of magnitude faster than in quartz, but is less well constrained than quartz, mostly due to the large variability reported for calcite reaction rate constants measurements. Taking a middle value for $v_s = 0.01 - 0.1m/Myr$ of calcite, the time to grow a stylolite with $L = 1$ cm 'teeth' is predicted to take typically $t_d \approx 1 - 0.1$ Myr in carbonates. Assuming a burial rate of about 10 Myr/km, it follows that sediments can be buried down to ~ 100 meters in 1 Myr, which implies that stylolites in carbonates can be observed already at tens to a hundred meters depth. This calculation suggests an alternative explanation for the minimum depth below which stylolites may develop: Instead of being initiated only by large enough overburden stress and temperature, stylolitic appearance may be controlled by the duration of formation, t_d. A continuous formation process agrees with observations in ODP cores where pelagic sediments show that stylolites develop continuously with depth [*Lind*, 1993].

In this study, we have neglected the effect of gravity on the collapse velocity. This effect is however important in geological settings, thus it would be relevant to further study the evolution of concentration and porosity fields in the presence of gravity acting in the direction of chemical compaction.

It is an interesting question whether the effect of clays, through heterogeneous equilibrium concentrations, leads to an interfacial instability. It might be that stylolites are formed in the presence of clay by a combination of the Mullins Sekerka (MS) instability [*Mullins and Sekerka*, 1963] and the reactive infiltration (RI) instability [*Spiegelman et al.*, 2001]. A MS instability occurs when a crystal is embedded in a bath of cold (or supersaturated) liquid, and the crystal surface grows due to local solidification, while the bulk liquid is mechanically and chemically inert. Therefore, the constitutive equations are Laplacian or diffusion-dominated, whereas, in the present scenario, there is an effective bulk precipitation in the porous media, which gives an additional source term. The RI instability occurs along a dissolution front in a porous media [*Chadam et al.*, 1986] or within the bulk porous rock in the presence of a solubility gradient *Aharonov et al.* [1997]. In reaction infiltration, the kinetics is controlled by the injection of reactive fluids, where fluid advection leads to the appearance of a reaction front and a morphological channeling instability. The reactive infiltration described in [*Aharonov et al.*, 1997] is in fact very similar to the one that may be induced by the presence of clay impurities, but it remains to be seen if it can be formed without advection, only in the presence of fluid diffusion.

Whether the difference to these two instabilities matter for the stability of the clay-layer would be an interesting subject of possible future work.

Acknowledgments. This study was supported by Physics of Geological Processes, a Center of Excellence at the University of Oslo and by the Danish VILLUM FOUNDATION.

Appendix: Numerical scheme

Eqs. (10)-(11) are stiff and nonlinear, hence numerical stability and accuracy of the discretization scheme need special treatment. Hereby, we integrate numerically the above equations using an implicit scheme similar to one used in Ref. ([*Zhao et al.*, 2008]). The porosity $\phi(x,t)$ and concentration $u(x,t)$ are defined on a 1D lattice at position j and time n by $\phi_{j,n}$ and $u_{j,n}$. Then, the evolution of $\phi_{j,n+1}$ is described by a set of coupled maps obtained by discretizing Eq. (10) as follows

$$\left(\frac{1}{dt} + \epsilon u_{j,n+1} + v_s \nabla\right) \phi_{j,n+1} = \frac{\phi_{j,n}}{dt}, \tag{20}$$

where the advection part is solved by the second order upwind scheme. Since $v_s < 0$, we use

$$\nabla \phi_{j,n+1} \equiv \frac{4\phi_{j+1,n+1} - \phi_{j+2,n+1} - 3\phi_{j,n+1}}{2dx}. \tag{21}$$

The map for $u_{j,n+1}$ is obtained from Eq. (11) and given by

$$\left(\frac{\phi_{j,n+1}}{dt} - L_{i,j}^{n+1}[\phi] + \phi_{j,n+1}\right) u_{j,n+1} = \frac{\phi_{j,n} u_{j,n}}{dt}, \tag{22}$$

where $L_{i,j}[\phi] = dx^{-2}(\phi_{j+1}^3 \delta_{i,j+1} + \phi_{j-1}^3 \delta_{i,j-1} - (\phi_{j+1}^3 + \phi_{j-1}^3)\delta_{i,j})$. From Eq. (22), $u_{j,n+1}$ is obtained as the solution $A^{-1}B$ of the matrix equation $Au = B$ with A and B defined from Eq. (22). The boundary condition is $x = 0$ is set as

$$A_{1,1} = -\frac{\phi_1^2}{dx} - \frac{\beta}{\epsilon}, \quad A_{1,2} = \frac{\phi_2^2}{dx}, \quad B_1 = -\frac{\beta}{\epsilon}\Delta, \tag{23}$$

and $A_{1,j} = 0$ for $j > 2$ and $B_j = 0$ for $j > 1$. The condition at infinity is set by $A_{N,N} = 1$ and $A_{N,j} = 0$ for $j < N$, where N is the linear system size.

After each update we generate the new fields $\phi^k_{j,n+1}$ and $u^k_{j,n+1}$ and the system of Eqs. (20)-(22) is iterated with the updated fields until the solution converges to the fixed points $\phi^k_{j,n+1} = \phi^{k-1}_{j,n+1} = \phi_{j,n+1}$ and $u^k_{j,n+1} = u^{k-1}_{j,n+1} = u_{j,n+1}$. We iterate Eqs. (20)-(22) until the convergence error $E = Max\,(E_\phi, E_u)$, with $E_\phi = \sqrt{\sum_j (\phi^k_{j,n+1} - \phi^{k-1}_{j,n+1})}$ and $E_u = \sqrt{\sum_j (u^k_{j,n+1} - u^{k-1}_{j,n+1})}$, is below a threshold $E \leq e_0 \ll 1$.

References

Aharonov, E., and R. Katsman, Interaction between pressure solution and clays in stylolite development: Insights from modeling, *American Journal of Science*, *309*(7), 607, 2009.

Aharonov, E., M. Spiegelman, and P. Kelemen, Three-dimensional flow and reaction in porous media: Implications for the earth's mantle and sedimentary basins, *Journal of Geophysical Research*, *102*, 14–14, 1997.

Angheluta, L., E. Jettestuen, J. Mathiesen, F. Renard, and B. Jamtveit, Stress-driven phase transformation and the roughening of solid-solid interfaces, *Physical review letters*, *100*(9), 96,105, 2008.

Angheluta, L., J. Mathiesen, C. Misbah, and F. Renard, Morphological instabilities of stressed and reactive geological interfaces, *Journal of Geophysical Research*, *115*(B6), B06,406, 2010.

Arvidson, R., I. Ertan, J. Amonette, and A. Luttge, Variation in calcite dissolution rates::: A fundamental problem?, *Geochimica et Cosmochimica Acta*, *67*(9), 1623–1634, 2003.

Bjorkum, P., How important is pressure in causing dissolution of quartz in sandstones?, *Journal of Sedimentary Research*, *66*(1), 147, 1996.

Chadam, J., D. Hoff, E. Merino, P. Ortoleva, and A. Sen, Reactive infiltration instabilities, *IMA journal of applied mathematics*, *36*(3), 207–221, 1986.

Coto, B., C. Martos, J. Peña, R. Rodríguez, and G. Pastor, Effects in the solubility of caco¡ sub¿ 3¡/sub¿: Experimental study and model description, *Fluid Phase Equilibria*, 2012.

Dewers, T., and P. Ortoleva, A coupled reaction/transport/mechanical model for intergranular pressure solution, stylolites, and differential compaction and cementation in clean sandstones, *Geochimica et Cosmochimica Acta*, *54*(6), 1609–1625, 1990.

Dysthe, D., R. Wogelius, C. Tang, and A. Nield, Evolution of mineral–fluid interfaces studied at pressure with synchrotron x-ray techniques, *Chemical geology*, *230*(3), 232–241, 2006.

Ebner, M., D. Koehn, R. Toussaint, and F. Renard, The influence of rock heterogeneity on the scaling properties of simulated and natural stylolites, *Journal of Structural Geology*, *31*(1), 72–82, 2009.

Emmanuel, S., J. Ague, et al., Modeling the impact of nano-pores on mineralization in sedimentary rocks, *Water Resour. Res*, *45*, W04,406, 2009.

Emmanuel, S., J. Ague, and O. Walderhaug, Interfacial energy effects and the evolution of pore size distributions during quartz precipitation in sandstone, *Geochimica et Cosmochimica Acta*, 2010.

Fletcher, R., and D. Pollard, Anticrack model for pressure solution surfaces, *Geology*, *9*(9), 419, 1981.

Fueten, F., P. Robin, and M. Schweinberger, Finite element modelling of the evolution of pressure solution cleavage, *Journal of structural geology*, *24*(6-7), 1055–1064, 2002.

Gal, D., A. Nur, and E. Aharonov, Stability analysis of a pressure-solution surface, *Geophysical research letters*, *25*(8), 1237–1240, 1998.

Greene, G., K. Kristiansen, E. Meyer, J. Boles, and J. Israelachvili, Role of electrochemical reactions in pressure solution, *Geochimica et Cosmochimica Acta*, *73*(10), 2862–2874, 2009.

Heald, M., Significance of stylolites in permeable sandstones, *Journal of Sedimentary Research*, *29*(2), 251–253, 1959.

Hem, J., *Study and interpretation of the chemical characteristics of natural water*, vol. 2254, Dept. of the Interior, US Geological Survey, 1985.

Hickman, S., and B. Evans, Kinetics of pressure solution at halite-silica interfaces and intergranular clay films, *Journal of Geophysical Research*, *100*(B7), 13,113, 1995.

Katsman, R., E. Aharonov, and H. Scher, A numerical study on localized volume reduction in elastic media: Some insights on the mechanics of anticracks, *Journal of Geophysical Research*, *111*(B3), B03,204, 2006.

Koehn, D., F. Renard, R. Toussaint, and C. Passchier, Growth of stylolite teeth patterns depending on normal stress and finite compaction, *Earth and Planetary Science Letters*, *257*(3-4), 582–595, 2007.

Kristiansen, K., M. Valtiner, G. Greene, J. Boles, and J. Israelachvili, Pressure solution–the importance of the electrochemical surface potentials, *Geochimica et Cosmochimica*

Acta, 2011.

Laronne Ben-Itzhak, L., E. Aharonov, R. Toussaint, and A. Sagy, in press, *Earth and Planetary Science Letters*, 2012.

Lind, I., Stylolites in chalk from leg 130, ontong java plateau, in *Proceedings of the Ocean Drilling Program, scientific results*, vol. 130, pp. 445–451, 1993.

Marshak, S., and T. Engelder, Development of cleavage in limestones of a fold-thrust belt in eastern New York, *Journal of Structural Geology*, *7*(3-4), 345–359, 1985.

McClay, K., Pressure solution and Coble creep in rocks and minerals: a review, *Journal of Geological Society*, *134*(1), 57, 1977.

Merino, E., P. Ortoleva, and P. Strickholm, Generation of evenly-spaced pressure-solution seams during (late) diagenesis: A kinetic theory, *Contributions to Mineralogy and Petrology*, *82*(4), 360–370, 1983.

Misbah, C., F. Renard, J. Gratier, K. Kassner, et al., Dynamics of a dissolution front for solids under stress, *Geophys. Res. Lett*, *31*, L06,618, 2004.

Mullins, W., and R. Sekerka, Morphological Stability of a Particle Growing by Diffusion or Heat Flow, *Journal of Applied Physics*, *34*, 323, 1963.

Oelkers, E., P. Bjorkum, and W. Murphy, A petrographic and computational investigation of quartz cementation and porosity reduction in North Sea sandstones, *American Journal of Science*, *296*(4), 420, 1996.

Renard, F., P. Ortoleva, and J. Gratier, Pressure solution in sandstones: influence of clays and dependence on temperature and stress, *Tectonophysics*, *280*(3-4), 257–266, 1997.

Renard, F., J. Gratier, and B. Jamtveit, Kinetics of crack-sealing, intergranular pressure solution, and compaction around active faults, *Journal of Structural Geology*, *22*(10), 1395–1407, 2000.

Renard, F., D. Dysthe, J. Feder, K. Bjørlykke, and B. Jamtveit, Enhanced pressure solution creep rates induced by clay particles: Experimental evidence in salt aggregates, *Geophysical Research Letters*, *28*(7), 1295–1298, 2001.

Rutter, E., Pressure solution in nature, theory and experiment, *Journal of Geological Society*, *140*(5), 725, 1983.

Rutter, E., and P. Wanten, Experimental study of the compaction of phyllosilicate-bearing sand at elevated temperature and with controlled pore water pressure, *Journal of Sedimentary Research*, *70*(1), 107, 2000.

Safaricz, M., and I. Davison, Pressure solution in chalk, *AAPG bulletin*, *89*(3), 383, 2005.

Schmittbuhl, J., F. Renard, J. Gratier, and R. Toussaint, Roughness of stylolites: implications of 3d high resolution topography measurements, *Physical review letters*, *93*(23), 238,501, 2004a.

Schmittbuhl, J., F. Renard, J. Gratier, and R. Toussaint, Roughness of stylolites: implications of 3d high resolution topography measurements, *Physical Review Letters*, *93*(23), 238,501, 2004b.

Sibley, D., and H. Blatt, Intergranular pressure solution and cementation of the Tuscarora orthoquartzite, *Journal of Sedimentary Research*, *46*(4), 881, 1976.

Spiegelman, M., P. Kelemen, and E. Aharonov, Causes and consequences of flow organization during melt transport: The reaction infiltration instability in compactible media, *Journal of Geophysical Research*, *106*(B2), 2061–2077, 2001.

Steefel, C., and A. Lasaga, A coupled model for transport of multiple chemical species and kinetic precipitation/dissolution reactions with applications to reactive flow in single phase hydrothermal systems, *American Journal of Science*, *294*(5), 529–592, 1994.

Tada, R., and R. Siever, Pressure solution during diagenesis, *Annual Review of Earth and Planetary Sciences*, *17*, 89, 1989.

Thomson, A., Pressure solution and porosity, *Silica in sediments: SEPM Special Publication*, *7*, 92–110, 1959.

Walderhaug, O., and P. Bjorkum, The effect of stylolite spacing on quartz cementation in the lower Jurassic Sto Formation, southern Barents Sea, *Journal of Sedimentary Research*, *73*(2), 146, 2003.

Walderhaug, O., E. Oelkers, and P. Bjorkum, An Analysis of the Roles of Stress, Temperature, and pH in Chemical Compaction of Sandstones: Discussion, *Journal of Sedimentary Research*, *74*(3), 447, 2004.

Walderhaug, O., P. Bjorkum, and N. Aase, Kaolin-Coating of Stylolites, Effect on Quartz Cementation and General Implications for Dissolution at Mineral Interfaces, *Journal of Sedimentary Research*, *76*(2), 234, 2006.

Wangen, M., Modeling porosity evolution and cementation of sandstones, *Marine and petroleum geology*, *15*(5), 453–465, 1998.

Wangen, M., Modelling quartz cementation of quartzose sandstones, *Basin Research*, *11*, 113–126, 1999.

Weyl, P., Pressure solution and the force of crystallizationa phenomenological theory, *Journal of Geophysical Research*, *64*(11), 2001–2025, 1959.

Yasuhara, H., C. Marone, and D. Elsworth, Fault zone restrengthening and frictional healing: The role of pressure solution, *Journal of Geophysical Research*, *110*, B06,310, 2005.

Zhao, C., B. Hobbs, P. Hornby, A. Ord, S. Peng, and L. Liu, Theoretical and numerical analyses of chemical-dissolution front instability in fluid-saturated porous rocks, *International Journal for Numerical and Analytical Methods in Geomechanics*, *32*(9), 1107–1130, 2008.

Parameters	Quartz	Calcite
c_{eq}^{∞}	$0.6 - 60 \times 10^{-5}$,	$4 - 100 \times 10^{-5}$
ϕ_{∞}	0.2	0.2
k_b [m/s]	10^{-10}	$10^{-9} - 10^{-6}$
k_i [m/s]	10^{-9}	$10^{-8} - 10^{-5}$
A_b [m^{-1}]	100	100
A_i	$1 - 100$	$1 - 100$
D_0 [m^2/s]	10^{-9}	10^{-9}
ρ_s [kg/m^3]	2650	2710
R_b^0 [kg/(m^3 s)]	2.6×10^{-5}	$2.7 \times 10^{-4} - 10^{-1}$
R_i^0 [kg/(m^2 s)]	$2.6 \times 10^{-6} - 10^{-4}$	$2.7 \times 10^{-5} - 10^{0}$

Table 1. Typical rock parameter values for quartz [*Merino et al.*, 1983; *Wangen*, 1998] and calcite [*Arvidson et al.*, 2003].

Figure 1. (Color online). The steady state porosity ϕ (panel (a)) and concentration u (panel (b)) plotted as functions of the distance to the stylolite surface x in units of x_0 ($x_0 \sim 0.2$ m for quartz and $x_0 \sim 10^{-2} - 10^{-1}$ m for calcite) for different values of β and Δ. Since the far-field porosity ϕ_0 is uniform, we have superimposed a Gaussian peak of higher porosity so that the amount of collapsed solid can be estimated by how much the peak has moved as seen in panel (a). The asymptotic steady state solution of the porosity is characterized by a profile that is independent of β and Δ, but with different collapse rates as given by the final position of the high porosity Gaussian peak. Also the concentration u has an universal decay away from the interface, but its value at the reactive surface, $u(x = 0)$, depends strongly on β and Δ. However, by rescaling the concentration field with the far-field analytical solution $u(0) \exp(-x/\phi_0)$, we find that the data collapses onto the same curve as shown in panel (b).

Figure 2. (Color online). Comparison between field measurements of the porosity profile in sandstone taken from Ref. [*Emmanuel et al.*, 2010] and the numerical solution of the steady state porosity ϕ. We use typical parameter values for quartz namely $\epsilon = 4 \times 10^{-5}$, $\phi_0 = 0.2$, $b = 1$, $\Delta = 0.01$ and $\beta = 1.6 \times 10^{-4}$. However, we notice that the stationary $\phi(x)$ is robust to different values of Δ and β, but with different relaxation timescales to the steady state.

Figure 3. (Color online). Relaxation to a steady state regime with a constant velocity of collapse v_s. Snapshots of the porosity profile at several times is shown in panel (a) and the corresponding concentration is presented in panel (b) as functions of the distance x (measured in units of x_0) from the dissolution interface. The profiles become stationary after about 10^6 of the typical time units t_0 (in real units 10^6 yr) for a relative supersaturation of $\Delta = 0.01$. The evolution of velocity v_s as a function of time is shown in the inset plot in panel a). The parameter values for the simulation are $\epsilon = 4 \times 10^{-5}$, $\phi_0 = 0.2$, $b = 1$, $\Delta = 0.01$ and $\beta = 2 \times 10^{-4}$.

Figure 4. (Color online). Velocity v_s (measured in units of $v_0 \sim 0.2$ m/yr for quartz and of $v_0 \sim 10^{-2} - 10^2$ m/yr for calcite) as a function of β and Δ. In panel (a), the $|v_s|$ is plotted versus β for different values of Δ, where we see that $|v_s|$ increases with β and Δ and, eventually, at larger values becomes independent of both. The dependence on both variables is shown in the two-dimensional contour plot in panel (b).

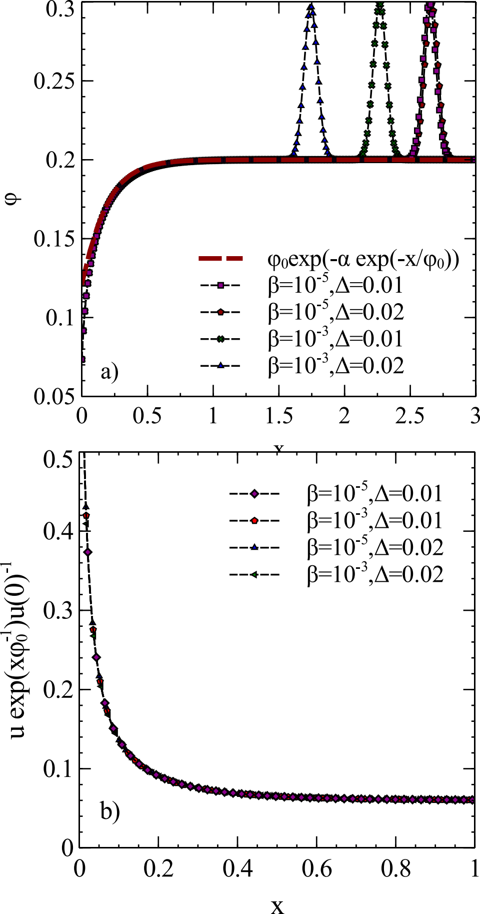
0.3
0.25
0.2
0.15
0.1
0.05
φ
$\varphi_0\exp(-\alpha\exp(-x/\varphi_0))$
$\beta=10^{-5},\Delta=0.01$
$\beta=10^{-5},\Delta=0.02$
$\beta=10^{-3},\Delta=0.01$
$\beta=10^{-3},\Delta=0.02$
a)
0
0.5
1
1.5
2
2.5
3
x
0.5
0.4
0.3
0.2
0.1
0
$u\exp(x\varphi_0^{-1})u(0)^{-1}$
$\beta=10^{-5},\Delta=0.01$
$\beta=10^{-3},\Delta=0.01$
$\beta=10^{-5},\Delta=0.02$
$\beta=10^{-3},\Delta=0.02$
b)
0
0.2
0.4
0.6
0.8
1
x

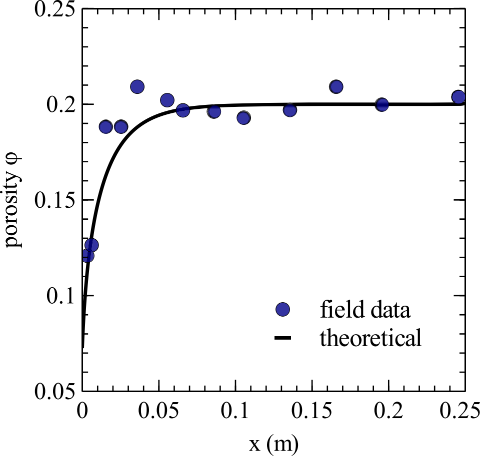
0.25
0.2
0.15
0.1
0.05
porosity φ
0
0.05
0.1
0.15
0.2
0.25
x (m)
field data
theoretical

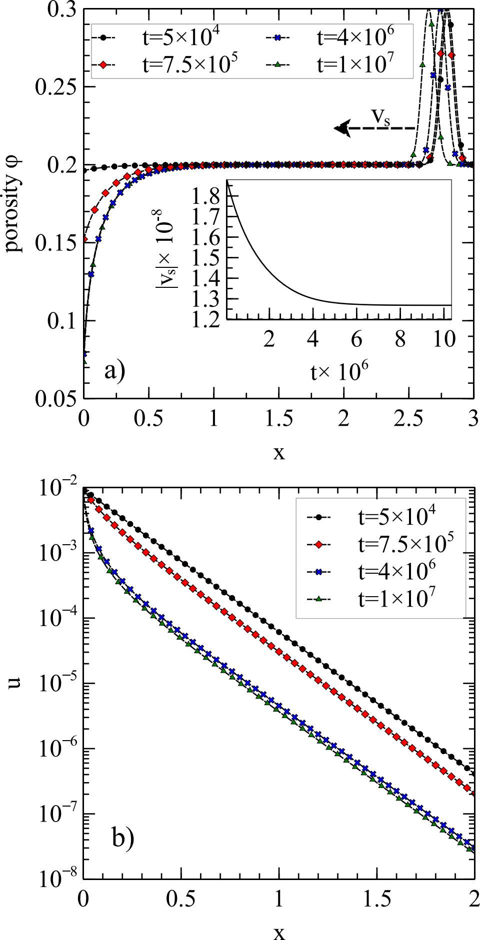
t=5×10^4
t=7.5×10^5
t=4×10^6
t=1×10^7
v_s
porosity φ
0.3
0.25
0.2
0.15
0.1
0.05
|v_s|× 10^-8
1.8
1.7
1.6
1.5
1.4
1.3
1.2
2
4
6
8
10
t× 10^6
a)
0
0.5
1
1.5
2
2.5
3
x
10^-2
10^-3
10^-4
10^-5
10^-6
10^-7
10^-8
u
t=5×10^4
t=7.5×10^5
t=4×10^6
t=1×10^7
b)
0
0.5
1
1.5
2
x

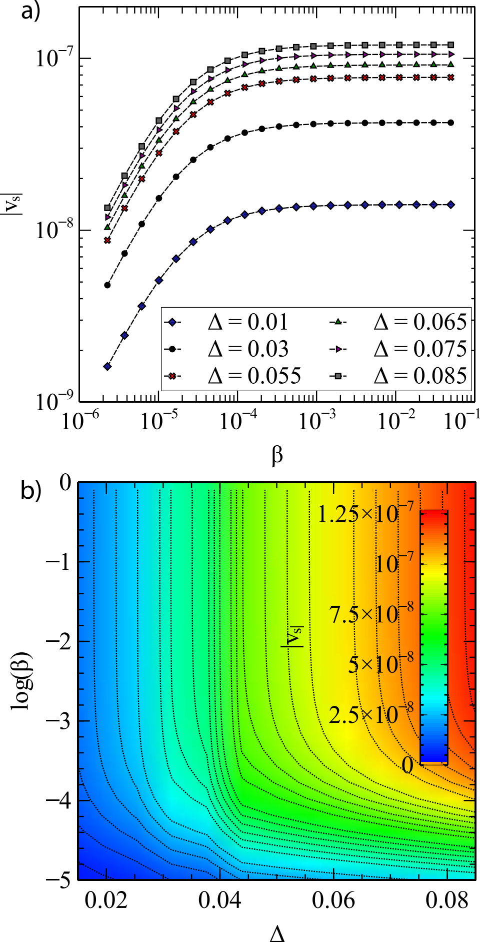
a)
10^{-7}
10^{-8}
10^{-9}
$|v_s|$
$\Delta = 0.01$
$\Delta = 0.03$
$\Delta = 0.055$
$\Delta = 0.065$
$\Delta = 0.075$
$\Delta = 0.085$
10^{-6}
10^{-5}
10^{-4}
10^{-3}
10^{-2}
10^{-1}
β
b)
0
−1
−2
−3
−4
−5
log(β)
1.25×10^{-7}
10^{-7}
7.5×10^{-8}
5×10^{-8}
2.5×10^{-8}
0
$|v_s|$
0.02
0.04
0.06
0.08
Δ